Eosin Yellow Dye Adsorption from Aqueous Solution Using Native Maize Husk

Ayomide Ogundipe,[a] Adesola Babarinde,[a] Ali El-Rayyes,[b] Amnah Mohammed Alsuhaibani,[c] Moamen S. Refat,[d] and Edwin Andrew Ofudje [e]

This work examines the uptake of Eosin Yellow (EY), an anionic dye, from aqueous solution using native maize (*Zea mays*) husk (MH) as a biosorbent. The biomass was characterized using Brunauer–Emmett–Teller (BET), Fourier transform infrared spectroscopy (FT-IR), and scanning electron microscopy (SEM), revealing a mesoporous structure and the presence of hydroxyl, carboxyl, and aromatic functional groups. Batch adsorption experiments were performed to assess the effects of contact time, pH, initial dye concentration, and adsorbent dosage. Maximum removal efficiency of 90.3% was attained at 1.5 g adsorbent dosage, pH 2, and 60-min contact time. The Langmuir isotherm best described the equilibrium data (R^2 = 0.957), with a maximum adsorption capacity of 44.5 mg g^{-1}. Kinetic data were adequately described by multiple empirical models, suggesting complex uptake behavior; however, no single rate-controlling mechanism was definitively established. Information from thermodynamic constants ($\Delta G° < 0$, $\Delta H° = 21.0$ kJ mol^{-1}, $\Delta S° = 9.25$ J mol^{-1} K^{-1}) signify that the adsorption process was spontaneous and endothermic, with features consistent with physisorption. Regeneration investigations revealed that the adsorbent retained appreciable performance over multiple cycles. These results revealed that maize husk is a promising biosorbent for dye removal under controlled laboratory conditions, although further studies are required to assess its performance in complex wastewater systems and at larger scales.

DOI: 10.15376/biores.21.3.6267-6296

Keywords: Anionic dye; Regeneration; Remediation; Thermodynamics; Wastewater

Contact information: a: Department of Chemistry, Olabisi Onabanjo University, Ago-Iwoye, Ogun State, Nigeria; b: Center for Scientific Research and Entrepreneurship, Northern Border University, 73213, Arar, Saudi Arabia; c: Department of Sports Health, College of Sport Sciences & Physical Activity, Princess Nourah bint Abdulrahman University P.O. Box 84428, Riyadh 11671, Saudi Arabia, d: Department of Chemistry, College of Science, Taif University, P.O. Box 11099, Taif 21944, Saudi Arabia; e: Department of Chemical Sciences, Mountain Top University, Ibafo, Ogun State, Nigeria;
** Corresponding author: aogundipe04@gmail.com*

INTRODUCTION

Water is one of the most abundant and vital resources on earth, serving as a solvent for numerous biochemical and physicochemical processes. However, the degradation of water quality has emerged as a serious global concern, leading to life-threatening consequences for ecosystems and human health. In response, several countries have implemented strict measures to mitigate the misuse of wastewater discharged into water bodies.

Despite these efforts, large-scale pollution caused by industrial activities remains prevalent, particularly in developing and underdeveloped nations (Tariq and Mushtaq 2023). Industrial activities are among the primary contributors to water contamination, releasing effluents laden with hazardous and non-biodegradable substances (Ilyas *et al*. 2019). Industry discharges from the metal-processing sector contain highly stable inorganic and organic compounds, including heavy metals, while the textile and paint industries are major sources of synthetic dyes pollution in the water bodies (Kolya and Kang 2024). Other pollutants present in water bodies include agrochemicals, pesticide residues, pharmaceutical wastes, and domestic effluents from human activities (Fashae and Obateru 2021).

Synthetic dyes, such as those released from textile operations, are especially problematic because they persist in aquatic environments. They can greatly increase chemical oxygen demand (COD), reduce dissolved oxygen necessary for aquatic life, and block sunlight penetration, thus disrupting photosynthesis in aquatic plants (Periyasamy 2024). These ecological disturbances can lead to long-term imbalances in aquatic ecosystems. Additionally, these dyes often produce foul odours, worsen water quality, and harm nearby communities (Akhtar *et al*. 2021). Their toxic effects on humans are serious, potentially harming the liver, kidneys, reproductive systems, and central nervous system (Hemashenpagam and Selvajeyanthi 2023).

Eosin yellow (EY) is a synthetic anionic xanthene-based dye that is widely employed across multiple industrial sectors, including the manufacture of inks, pharmaceuticals, and various textile products (Das and Debnath 2021). Because of its vivid coloration, high stability, and resistance to light and chemical degradation, EY has become a preferred colorant in many applications. However, its widespread industrial usage has also raised significant environmental and health concerns. From a toxicological perspective, discharge of untreated EY dye into the water surface presents multiple risks to both humans and aquatic ecosystems. Direct exposure to the dye has been reported to cause eye and skin irritation, leading to inflammatory responses and potential allergic reactions in sensitive individuals (Adeoye *et al*. 2023). Beyond these acute effects, EY has been shown to interfere with protein–protein interactions, a process that can disrupt normal cellular functions and biochemical pathways (Al-Tohamy *et al.* 2022). It has also been revealed that EY exhibits genotoxic properties in humans, potentially inducing DNA damage that may contribute to mutagenesis and long-term health complications (Derayea and Nagy 2018). Given the significant toxicity of EY dye to both human health and aquatic ecosystems, there is an urgent need to develop effective treatment methods for wastewater contaminated with this dye.

In recent years, a wide range of treatment technologies have been explored for the removal of synthetic dyes from wastewater, which include advanced physical separation processes such as nanofiltration and reverse osmosis, adsorption, electrochemical methods, including electrolytic coagulation, and biological approaches, encompassing both aerobic and anaerobic treatments (Anfar *et al*. 2020; El-Rayyes *et al*. 2025). While these techniques can remove dye from wastewater, they are often limited by high capital and maintenance costs, complex operational procedures that increase overall expenses, and the generation of toxic by-products, which hinder their practical application especially in developing countries (Katibi *et al*. 2021). Among the various water treatment methods, adsorption stands out as a more suitable option due to its environmental friendliness, cost-effectiveness, operational simplicity, and robustness, which makes it efficiently applied

without generating any harmful by-products, and also an attractive choice for sustainable wastewater management (Hadad *et al*. 2019; Ofudje *et al*. 2024).

A variety of low-cost and naturally derived adsorbents have been investigated for the adsorption process, such as sugar cane peel (Ofudje *et al*. 2024), date palm seeds (Abdus-Salam *et al*. 2021), Cuban palm fruit pericarp (Adaramola *et al*. 2024), *Mangifera indica* leaves (Iqbal *et al*. 2023), wheat straw (Lin *et al*. 2017), teak leaf litter (Oyelude *et al*. 2017), and coffee wastes (Anastopoulos *et al*. 2017). Recent studies have continued to advance the development of efficient adsorbents for dye removal, with particular emphasis on low-cost and sustainable materials. For instance, biochar- and biomass-derived adsorbents have demonstrated promising performance due to their tunable surface properties and functional groups. Adeoye *et al.* (2023) reported the rapid removal of Eosin Yellow using zeolite-based materials, while Adaramola *et al.* (2024) demonstrated high adsorption capacity using Cuban palm fruit pericarp, albeit with additional processing requirements. Similarly, Song *et al*. (2023) investigated chemically treated corncob for Eosin Yellow removal, highlighting the role of surface modification in enhancing adsorption capacity. More recently, Pieczykolan (2025) and El-Rayyes *et al.* (2025) emphasized the importance of combining kinetic, isotherm, and thermodynamic analyses to better understand adsorption mechanisms in biomass-derived systems.

Maize (*Zea mays*) is a staple crop that serves as a primary food source for billions of people worldwide, providing essential nutrients such as carbohydrates and proteins (Elisa *et al*. 2022). The maize husk (MH), which forms the leafy outer covering of the corn ear, is generated in large quantities as an agricultural by-product during maize production (Sharma *et al*. 2019). Although often discarded or underutilized, research has demonstrated that MH can be repurposed for diverse applications such as a biosorbent for heavy metal removal and as a raw material for activated carbon production, mushroom cultivation substrates, and bioethanol synthesis (Biswas 2022). Given its abundance, low cost, biodegradability, and promising adsorption potential, MH represents a sustainable and environmentally friendly resource for wastewater treatment.

With much research focusing on low-cost adsorbents for dye removal, some limitations remain unresolved. A majority of studies have focused on chemically or thermally modified adsorbents including functionalized biochars, activated carbons, or composite adsorbents, which often exhibit enhanced adsorption performance. Nevertheless, these modifications often involve additional processing steps, chemical inputs, and energy consumption, which increases the cost and limits practical applicability, most especially in resource-constrained settings. On the other hand, comparatively fewer findings have systematically examined the adsorption performance of native (unmodified) lignocellulosic biomass under well-defined conditions. This signifies a critical gap, as baseline performance data are necessary to evaluate whether modification strategies are truly justified or whether acceptable adsorption efficiency can be obtained using minimally processed materials. The relative advantages of more complex adsorbents remain difficult to quantify without such benchmarks. Moreover, although maize-derived materials such as husk-based activated carbon, and corncob have been tested for pollutant removal, the intrinsic adsorption behavior of raw maize husk in its native form has not been sufficiently established for specific dye systems such as Eosin Yellow. Given that adsorption performance is highly dependent on adsorbate chemistry and surface interactions, extrapolation from other dyes or modified materials is not always reliable.

Though equilibrium capacity is reported in most adsorption studies, few studies have assessed the reusability of biosorbents over multiple cycles, which is an important factor for assessing their practical viability. Furthermore, mechanistic interpretations in adsorption studies are usually obtained directly from empirical kinetic or isotherm model fitting, without adequate consideration of their limitations. This causes overinterpretation of adsorption pathways without independent verification of transport or surface interaction processes. As a result of these gaps, the present work aims to provide a systematic evaluation of native maize (*Zea mays*) husk as a minimally processed biosorbent for the adsorption of Eosin Yellow from aqueous solution. The work focuses on (i) establishing baseline adsorption performance under different operational parameters, (ii) evaluating equilibrium, kinetic, and thermodynamic behavior, and (iii) evaluating regeneration potential over multiple adsorption–desorption cycles. By emphasizing a low-processing approach and critically interpreting the results, this study contributes to a more realistic assessment of biomass-derived adsorbents for potential environmental applications.

MATERIALS AND METHODS

Materials

The maize husk (*Zea mays*) used in this study was sourced from new market, Ijebu-Ode, Ogun State, Nigeria. Analytical grade Eosin yellow dye (molecular formula: $C_{20}H_6Br_4Na_2O_5$; molecular weight: 691.85 g/mol; Fig. 1) was procured from Sigma-Aldrich, United Kingdom. All reagents employed in the study were of analytical grade, and double-distilled water was used for all experimental preparations and procedures.

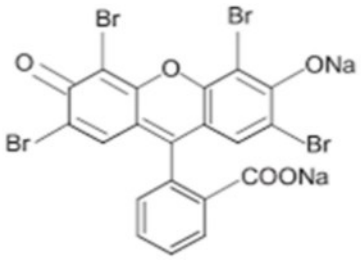


Fig. 1. Molecular structure of Eosin yellow dye

Methods

Adsorbent preparation

The maize husk employed in this study was obtained from a local market in Ijebu-Ode, Ogun State, Nigeria. The biomass was manually sorted to eliminate visible impurities such as dust, dirt, and foreign plant matter before processing. The raw material was carefully washed with double-distilled water in multiple cycles until the wash water appeared clear, so as to eliminate adhering soil particles and soluble contaminants. The washed material was then air-dried under ambient laboratory conditions (25 ± 2 °C) for seven days until a constant weight was obtained, ensuring adequate moisture elimination without thermal degradation of the lignocellulosic structure. The dried maize husk was then reduced in size using a locally fabricated mechanical grinding and milling machine. The ground material was sieved using a fine mesh sieve with a nominal aperture size of 20 µm**,** and the fraction passing through the sieve was collected for use in adsorption experiments. It should be noted that this value represents the maximum particle size**,** and the resulting

material consists of a distribution of particles smaller than 20 µm. The prepared adsorbent was stored in airtight containers at room temperature to minimize moisture uptake prior to use.

Preparation of Aqueous Dye Solutions

A stock solution of EY-dye was made by dissolving 1000 mg of the dye in 1000 mL of double-distilled water. Working solutions of concentrations in the range of 10 to 100 mg L^{-1} were obtained by serial dilution of EY stock solution. 0.1 M NaOH or 0.1 M HCl was used for the pH adjustment and measured with a pH meter (EcoSense pH100A, China). Dye absorbance was determined with a UV–Vis spectrophotometer (UV-1900, UK) at the maximum wavelength (λ_{max}) of 517 nm.

Adsorbent Characterization

The identification of the various functional groups present on the surface of the adsorbent was done *via* Fourier-transform infrared spectroscopy (Shimadzu FTIR-8400S, Japan) spectrophotometer. For sample preparation, 99% of the adsorbent mass was homogenized in an agate mortar with 01% of anhydrous KBr. The mixture was compressed into a transparent pellet using a Graseby Specac vacuum hydraulic press at 1.2 psi and scanned over the wavenumber range of 400 to 4000 cm^{-1}. The surface morphology and porosity of the adsorbent were examined using a scanning electron microscope (SEM, Phenom ProX, Eindhoven, Netherlands). Specific surface area and pore characteristics were analyzed using the Brunauer–Emmett–Teller (BET) instrument. Prior to analysis, the adsorbent was degassed under vacuum at 150 °C for 4 h to remove residual moisture and adsorbed impurities. Nitrogen adsorption–desorption isotherms were recorded at 77 K using a Micromeritics ASAP 2020 analyzer (USA). The point of zero charge (pH_{PZC}) was determined with a Zetasizer Nano ZS/Ultra (Malvern, UK).

Determination of Point of Zero Charge (pH_pzc)

The point of zero charge (pH_pzc) of the maize husk was determined using the pH drift method. A series of 50 mL electrolyte solutions (0.01 M NaCl) were prepared with initial pH values adjusted between 2 and 10 using 0.1 M HCl or 0.1 M NaOH. A fixed mass of adsorbent (0.1 g) was added to each solution and the suspensions were agitated for 24 h at room temperature to reach equilibrium. The final pH values were then recorded, and the pH_pzc was determined from the point where the curve of ΔpH ($pH_{final} - pH_{initial}$) versus $pH_{initial}$ intersects zero.

Batch Adsorption Studies

The capability of the MH in removing EY was investigated by analyzing the influence of significant experimental factors including pH, contact time, adsorbent dosage, and initial EY concentration. The batch adsorption was performed with a 50 mL dye solution contained inside 250 mL Erlenmeyer flasks with varying pH of 2 to 8, initial dye concentration of 10 to 100 mg/L, adsorbent dose values of 0.25 to 3.0 g and a contact time of 5 to 180 mins at 25 °C. The flasks holding the dye solution (100 mg/L) and the adsorbent (1.5 g) were completely shaken on the orbital shaking incubator at 200 rpm, 25 °C, within 240 mins, respectively. The adjustment of the pH of the reaction was done as previously mentioned. At predetermined agitation time, samples were withdrawn and then centrifuged (TGL-16A, British) at 2000 rpm for 10 min. Using the aliquots, the concentration of the

remaining EY dye was then determined. To calculate the quantity of EY adsorbed per unit mass and percentage dye removal, Eqs.1 and 2 were employed,

$$q_e = \frac{C_0 - C_e}{m} \times V \quad (1)$$

$$R(\%) = \frac{C_0 - C_e}{C_0} \times 100 \quad (2)$$

where q_e stands for the quantity of EY adsorbed, C_o (mg/L) and C_e is (mg/L) are the initial and equilibrium EY concentrations, V denotes the volume of EY (L) used, and m is the mass of the adsorbent (g).

Desorption Experiments

To evaluate the reusability of the adsorbent, desorption experiments were done with 0.2 M acetic acid as the desorbing agent. The spent adsorbent biomass underwent multiple adsorption–desorption cycles, and the percentage of dye recovered was computed to investigate the regeneration efficiency of the biomass using Eq. 3,

$$PD(\%) = \frac{AD}{AA} X100 \quad (3)$$

where AA and DA stand for the amount of dye adsorbed and the amount desorbed respectively. All experiments were done in triplicate, and the results represent the mean values with corresponding standard deviations.

Effect of Co-existing Ions

To assess the role of common co-existing ions on the adsorption performance of the prepared maize husk, batch adsorption experiments were conducted under previously optimized conditions. The experiments were performed at pH 2, adsorbent dosage of 1.5 g, contact time of 60 min, and an initial dye concentration of 100 mg/L. To simulate the presence of inorganic ions typically found in wastewater, selected salts were introduced into the dye solution at controlled concentrations. Sodium chloride (NaCl) was added at 0.01 M and 0.1 M to evaluate the effect of increasing ionic strength. In addition, calcium chloride ($CaCl_2$, 0.01 M) and sodium sulfate (Na_2SO_4, 0.01 M) were used to assess the influence of ion valency and type, representing monovalent (Na^+) and divalent (Ca^{2+}, SO_4^{2-}) ions. Each solution was prepared by dissolving the appropriate amount of salt in the dye solution prior to the addition of the adsorbent. The mixtures were agitated under constant conditions for 60 min to ensure equilibrium was reached. After adsorption, the suspensions were filtered, and the residual dye concentration was determined using a UV–Vis spectrophotometer. The percentage removal was calculated and compared with a control experiment conducted in the absence of added ions.

Adsorption Kinetics

The biosorption kinetics of EY dye onto MH were evaluated using three kinetic models which are Pseudo-First Order (PFO), Pseudo-Second Order (PSO), and Intra-Particle Diffusion (IPD). These models were applied to determine the adsorption kinetics and identify the rate-controlling mechanisms. The linearized forms of the PFO, PSO, and IPD equations at equilibrium were used, as expressed in Eqs. 4 to 6, respectively (Moussout *et al*. 2018; Revellame *et al*. 2020; Dharmarathna and Priyantha 2024):

$$\ln(q_e - q_t) = \ln q_e - K_1 t \quad (4)$$

$$\frac{t}{q_t} = \frac{1}{K_2 q_e^2} + \frac{t}{q_e} \quad (5)$$

$$q_t = K_{id} t^{\frac{1}{2}} + C \quad (6)$$

where the amount of EY adsorbed at time t (mg/g) is denoted as q_t, while the PFO rate constant (min^{-1}) is given as k_1, k_2 represent the PSO rate constant (g/mg·min), k_{id} stands for the IPD rate constant, and C denotes the intercept representing boundary layer thickness.

Adsorption Isotherm

The equilibrium data obtained at the solid – liquid interface was analyzed using three models, namely the Langmuir, Freundlich, and Temkin isotherms.

The Langmuir model's linearized equation is given as Eq. 7 (Vigdorowitsch *et al*. 2021):

$$\frac{C_e}{q_e} = \frac{C_e}{Q_{max}} + \frac{1}{Q_{max} K_L} \quad (7)$$

The Langmuir Separation Factor (R_L) is expressed as:

$$R_L = \frac{1}{(1 + bC_o)} \quad (8)$$

The amount of EY adsorbed (mg/g), and EY concentration remaining at equilibrium (mg/L) are given as q_e and C_e, the maximum adsorption capacity (mg/g) is denoted as q_m, while the Langmuir adsorption constant (L/mg) relating to the affinity of the binding sites is given as K_L.

The Freundlich isotherm describes multilayer adsorption on heterogeneous surfaces with varying affinities for the adsorbate and its linearized form is given as (El-Rayyes *et al*. 2025),

$$\log Q_e = \log k_f + \left(\frac{1}{n}\right) \log C_e \quad (9)$$

where k_f denotes the Freundlich adsorption coefficient (mg/g), and n is the Freundlich exponent related to the adsorption intensity.

The Temkin isotherm described the adsorbent–adsorbate interactions and assumes that the heat of sorption decreases linearly with rising coverage of the surface. Its linearized form is expressed as (Chu 2021):

$$q_e = \frac{RT}{b_\tau} \ln A_\tau + \frac{RT}{b_\tau} \ln C_e \quad (10)$$

The gas constant (8.314 J/mol·K) is given as R, absolute temperature (K) is T, while the Temkin heat of adsorption (J/mol) is given as b_T. The goodness of fit of each isotherm was evaluated based on the correlation coefficients (R^2) and error analysis as listed in Eq. 11 below (Aladag 2023):

$$\%SSE = \frac{\sum_i^n (q_e, cal. - q_e, cal)^2}{n} \times 100 \quad (11)$$

Thermodynamic Studies

Thermodynamic details were obtained for free energy change ($\Delta G°$), enthalpy change ($\Delta H°$), and entropy change ($\Delta S°$) by applying equations 12 to 14 (Batool *et al*. 2023; Liyanaarachchi *et al*. 2023),

$$K_d = {}^{q_e}/_{C_e} \quad (12)$$

$$\ln(\rho K_D) = -\frac{\Delta H}{RT} + \frac{\Delta S}{R} \quad (13)$$

$$\Delta G^{o} = RTInK_d \quad (14)$$

where the universal gas constant in 8.304 J $mol^{-1}K^{-1}$ is given as R, ρ is the water density (g/L) which was used to convert the equilibrium constant to dimensionless, and T denotes temperature in Kelvin.

RESULTS AND DISCUSSION

Adsorbent Characterization

Fourier transform infrared (FTIR) spectroscopy was employed to identify the functional groups present on the adsorbent surface before and after adsorption of Eosin Yellow, as shown in Fig. 2, while the summary is presented in Table 1. The spectrum of the raw maize husk exhibited characteristic bands associated with lignocellulosic materials with a broad band observed around 3124 to 3250 cm^{-1} that is assigned to O–H stretching vibrations of hydroxyl groups present in cellulose, hemicellulose, and lignin (Javier-Astete *et al*. 2021). Bands near 2918 cm^{-1} and 2845 cm^{-1}correspond to aliphatic C–H stretching vibrations, while those observed around 1645 to 1750 cm^{-1} is ascribed to aromatic C=C stretching or conjugated carbonyl groups. Those peaks in the region of 1075 to 1152 cm^{-1} are associated with the C–O stretching vibrations in alcohols, ethers, and esters (Javier-Astete *et al*. 2021).

Upon the uptake of Eosin Yellow, the FTIR spectrum displayed minor shifts in peak positions and changes in intensity for several bands, along with the appearance of additional features attributable to the dye molecules. Specifically, peaks assigned to O–H, C-H, C=C/C=O and C-O were seen in the regions of 3250-3550 cm^{-1}, 2945-2968 cm^{-1}, 1630-1775 cm^{-1} and 1072-1160 cm^{-1} respectively. These changes suggest that adsorption had occurred and that surface functional groups were involved in the interaction process. Nevertheless, it is important to emphasize that such spectral changes do not uniquely identify the type or dominance of specific interactions.

For EY-loaded MH, new peaks appear at 1552 cm^{-1} and 694 cm^{-1}, and this can be assigned to C=C stretching and C–Br vibrations of the EY-dye, respectively. The presence of these characteristic dye vibrations and shifts in the original biomass peaks suggest that adsorption occurred possibly *via* physical interactions in form of Van der Waals forces, hydrogen bonding, and π–π stacking between the aromatic structures of the dye and lignin, as well as possible electrostatic attractions at specific pH conditions (Abdus-Salam *et al*. 2021).

Table 1. FTIR Peak Assignment and Changes Before and After Adsorption

Wavenumber (cm^{-1}) – Before	Wavenumber (cm^{-1}) – After	Assignment	Observed Change	Interpretation (Conservative)
3124–3250	3250-3550	O–H stretching (hydroxyl groups)	Peak shift and intensity change	Suggest the involvement of hydroxyl-containing groups in adsorption
2845-2918	2945-2968	C–H stretching (aliphatic)	Slight intensity variation	Likely structural contribution, not directly indicative of interaction
1645-1750	1630-1775	C=C / C=O (aromatic or conjugated groups)	Peak shift	May reflect interaction with dye aromatic structure
1075-1152	1072-1160	C–O stretching (alcohol/ether)	Noticeable variation	Suggests participation of oxygen-containing functional groups
-	1552 cm^{-1} and 694	Dye-related functional groups	Appearance of additional bands	Confirms presence of adsorbed dye on surface

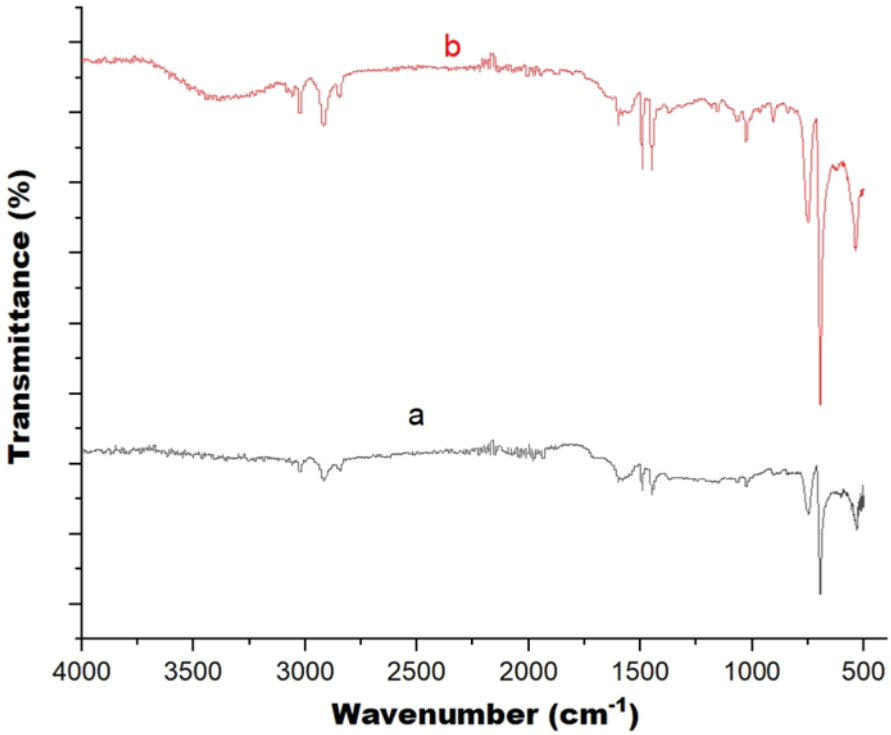


Fig. 2. FT-IR spectra of native maize husk before (a) and after adsorption (b)

The textural properties of the maize husk were evaluated using nitrogen adsorption–desorption analysis. The resulting isotherm (Fig. 3a) exhibits characteristics consistent with a Type I isotherm**,** according to IUPAC classification, indicating the presence of mesoporous structures. The BET specific surface area of the material was determined to be 105.3 m^2 g^{-1}**,** while the average pore diameter, obtained using the BJH method, was 2.8 to 3.0 nm**,** confirming that the pore system is predominantly within the mesopore range (2

to 50 nm) (Fig. 3b). The pore size distribution (Fig. 3c) shows a distinct peak centered around 2.5 nm, signifying a relatively narrow distribution of mesopores. The contribution of micropores (<2 nm) appeared limited, suggesting that adsorption was not dominated by micropore filling, but rather by adsorption on accessible internal surfaces. Mesopores facilitate the diffusion of relatively large dye molecules into the internal structure of the adsorbent, thus enhancing accessibility to adsorption sites. In the present study, the mesoporous nature of the maize husk likely contributed to the observed adsorption performance by reducing diffusion limitations. Nevertheless, the relatively fine particle size (<20 µm) used in batch experiments further enhanced mass transfer, and may partially account for the observed kinetics.

Such microporosity is advantageous for improving molecular diffusion and adsorption capacity, making MH–derived materials promising adsorbent for applications in adsorption, catalysis, and energy storage systems (Ismail *et al*. 2022).

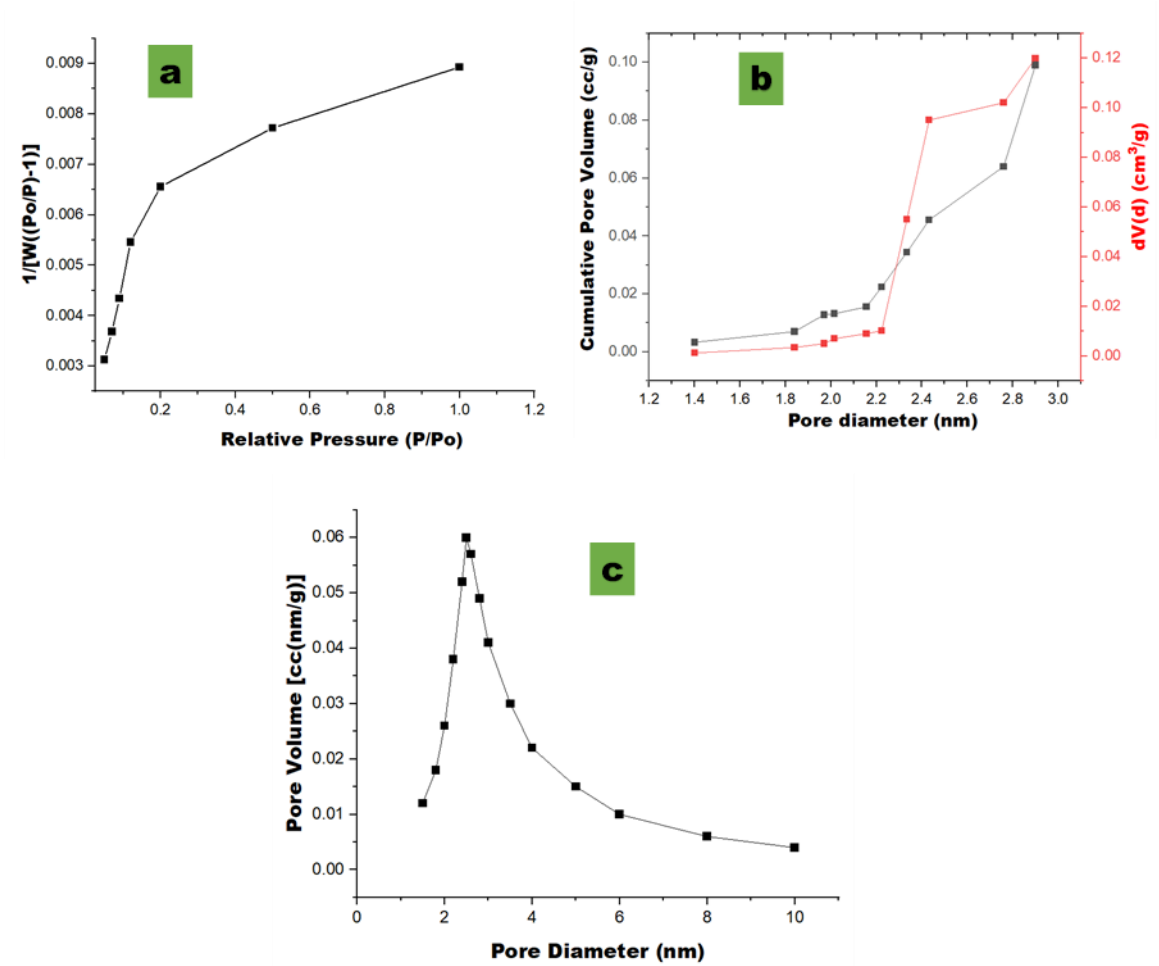


Fig. 3. Plots of (a) BET surface area, (b) cumulative pore volume distribution, and (c) pore size distribution curve analysis

The porous structure and surface morphology of unloaded-MH and EY-loaded MH as revealed by SEM images are presented in Figs. 4a and b, respectively. SEM was used to characterize the adsorbent's morphology and evaluate its surface features. The pronounced porosity of the adsorbent facilitates enhanced dye sorption onto its surface (Adeyemo *et al*. 2017). The unloaded-MH exhibited a irregular, rough, and highly porous surface with

numerous channels and cavities. These pores provide a large surface area and facilitate the movement of dye molecules into the internal adsorption sites which are primarily composed of cellulose, hemicellulose, and lignin frameworks that contribute to textural heterogeneity and surface roughness. After dye uptake (Fig. 4b), the surface became more compact and smoother. This noticeable reduction in visible pore openings and roughness may indicate that the dye had been successfully incorporated onto the surface and possibly penetrated the internal pores of the biomass matrix. The distinct structural alterations observed before and after adsorption underscore the critical role of adsorbent porosity in facilitating dye uptake (Mahmoodi *et al*. 2018).

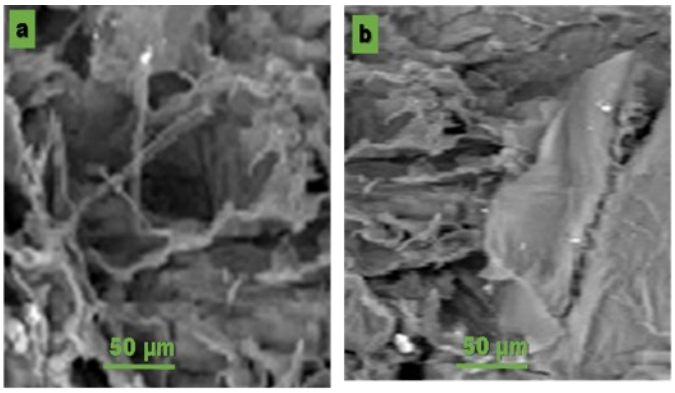


Fig. 4. SEM image of maize husk before (a) and after (b) EY adsorption

Impact of Adsorption Parameters on Adsorption

Effect of pH on sorption of EY dye

The pH of the dye solution is a critical parameter influencing the sorption of dyes, as it influences the protonation or deprotonation of the adsorbent's surface functional groups (Aragaw and Alene 2022). One critical parameter influencing adsorption behavior is the pH of the solution, as it affects both the surface charge of the adsorbent and the speciation of the adsorbate. In this study, the point of zero charge (pH_pzc) of the maize husk was determined to be 4.2, indicating that the adsorbent surface was positively charged at pH < 4.2 and negatively charged at pH > 4.2 (Fig. 5a). The adsorption results show that maximum dye removal occurs at pH 2 (Fig. 5b), which is significantly below the pH_pzc. Under these conditions, protonation of surface functional groups (*e.g*. carboxyl groups) leads to the development of a net positive surface charge (Lin *et al*. 2017). Since Eosin Yellow is an anionic dye under typical aqueous conditions, this creates favorable electrostatic attraction between the adsorbent surface and dye molecules. This strong correlation between pH_pzc and adsorption performance suggests that electrostatic interactions are a dominant driving force in the adsorption process, particularly under acidic conditions. As the pH increases toward and beyond the pH_pzc, the surface charge becomes less positive and eventually negative, resulting in reduced adsorption efficiency due to electrostatic repulsion (Soltani *et al*. 2021).

This behavior is consistent with many studies on adsorption of anionic dyes, where acidic pH favors adsorption. This has been reported by Mittal *et al*. (2013) and Ashur and Abbas (2020), where decreasing EY removal with increasing pH using de-oiled soya was documented. The work by Faria *et al*. (2004) confirms that anionic dye adsorption generally declines at higher pH because surface deprotonation leads to repulsion of dye anions. However, the observation that adsorption does not completely cease above the

pH_pzc indicates that electrostatic attraction is not the sole interaction mechanism**.** Residual adsorption at higher pH values suggests the possible contribution of non-electrostatic interactions, such as hydrogen bonding or π–π interactions between the aromatic structure of the dye and lignin components of the biomass. Nevertheless, it is important to emphasize that the present data do not allow quantitative separation of these contributions.

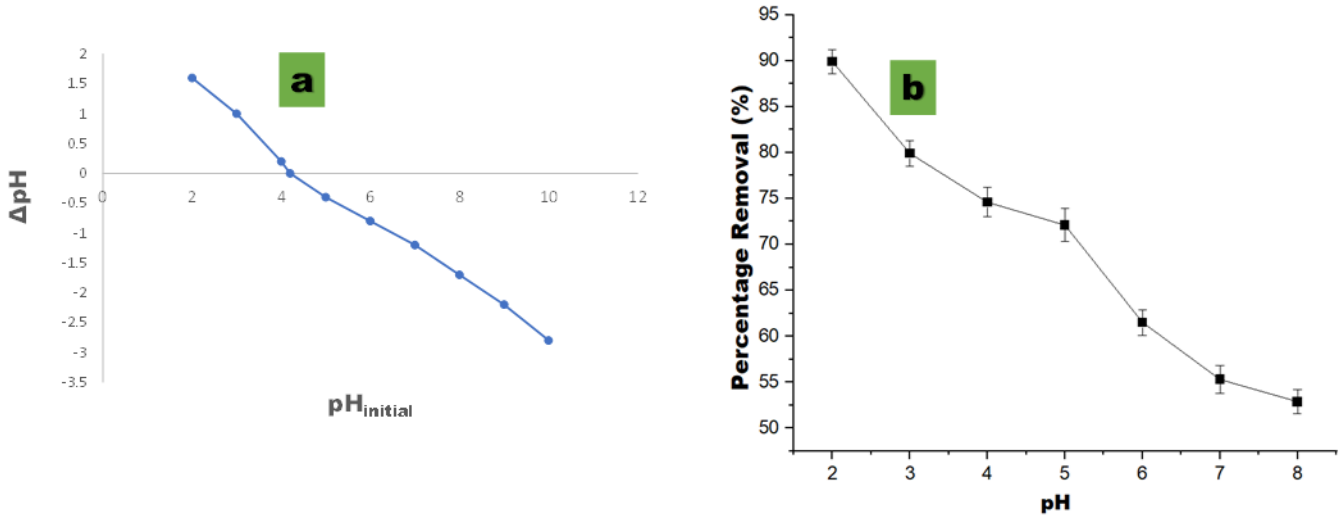


Fig. 5. Plots of (a) zero point charge of maize husk, and (b) impact of pH on the removal of EY using MH

Impact of Adsorbent Dosage on Adsorption

The adsorbent dosage is a key factor affecting the uptake process, as it determines the number of available active binding sites on the adsorbent surface for dye uptake (de Farias *et al*. 2020). To study this effect, varying amounts of MH ranging from 0.25 to 3.0 g were examined.

As shown in Fig. 6, the removal efficiency of EY surged with adsorbent dosage, attaining a maximum of 90% at 1.5 g. This trend is due to the greater number of available active sites for the contaminant uptake at higher dosages, which enhances dye uptake (Bernal *et al*. 2018). However, beyond the optimum dosage, the adsorption efficiency decreased as the dosage increased further. This decline is probably due to aggregation of particles at higher solid concentrations, which lessens the effective surface area and restricts the accessibility of active sites (Adeogun *et al*. 2018).

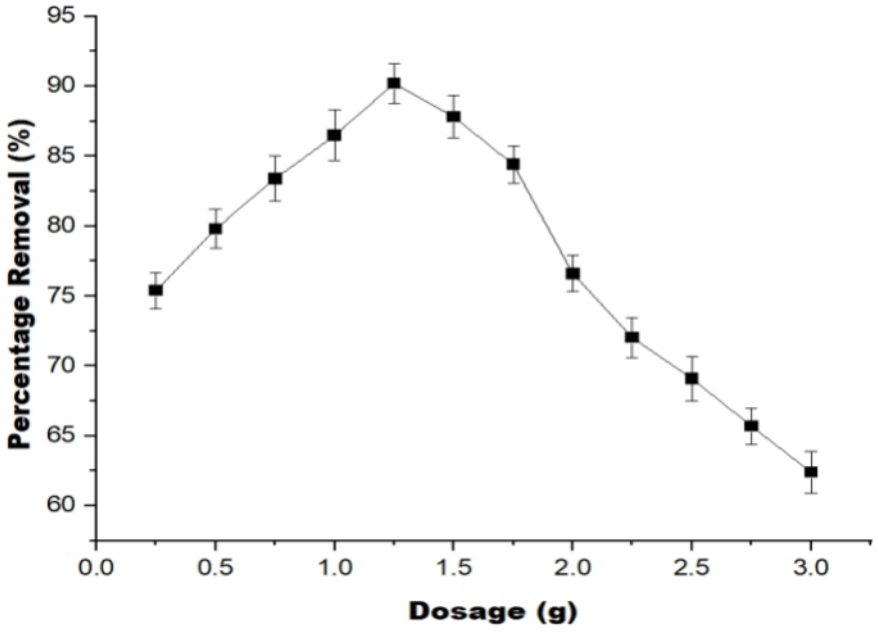


Fig. 6. Impact of MH dosage on the sorption of EY using MH

Impact of Initial EY Concentration

The impact of initial EY concentration on adsorption was studied using different concentrations from 10 to 100 mg/L, while keeping all other parameters constant, as shown in Fig. 7. From the plot, the amount adsorbed increased sharply with increasing EY concentration, reaching 45.2 mg/g at 80 mg/L, beyond which it leveled off. This trend suggests that higher EY concentrations offer a higher driving force for mass transfer between the adsorbent surface and the aqueous phase, improving adsorption until the available active sites approach saturation (Li and Zhai 2020; Adeoye *et al*. 2023). Conversely, the percentage removal decreased steadily with rising concentration. At low concentrations, most of the molecules of the dye can easily access the abundant active sites on the maize surface, resulting in higher removal efficiency. However, as the concentration rises, the adsorbent's active sites become saturated, resulting in reduced removal efficiency even though the amount adsorbed increases (Abdul-Salam *et al*. 2021).

This inverse relationship between adsorption capacity and removal percentage is a common behavior in batch adsorption systems and suggests that the sorption process is primarily controlled by surface site availability and diffusion effects at higher solute concentrations.

At low initial EY concentrations, a high percentage removal is achieved because the ratio of EY molecules to available adsorption sites is small, enhancing efficient capture of most molecules.

But when the concentration rises, although the absolute uptake per gram (q_e) rises (driven by a stronger concentration gradient and mass transfer driving force), the fraction of dye removed declines because the finite number of binding sites becomes increasingly saturated. This dual trend (rise in q_e but decrease in removal efficiency) is a well-documented behavior in batch adsorption of dyes (Rapo *et al*. 2021).

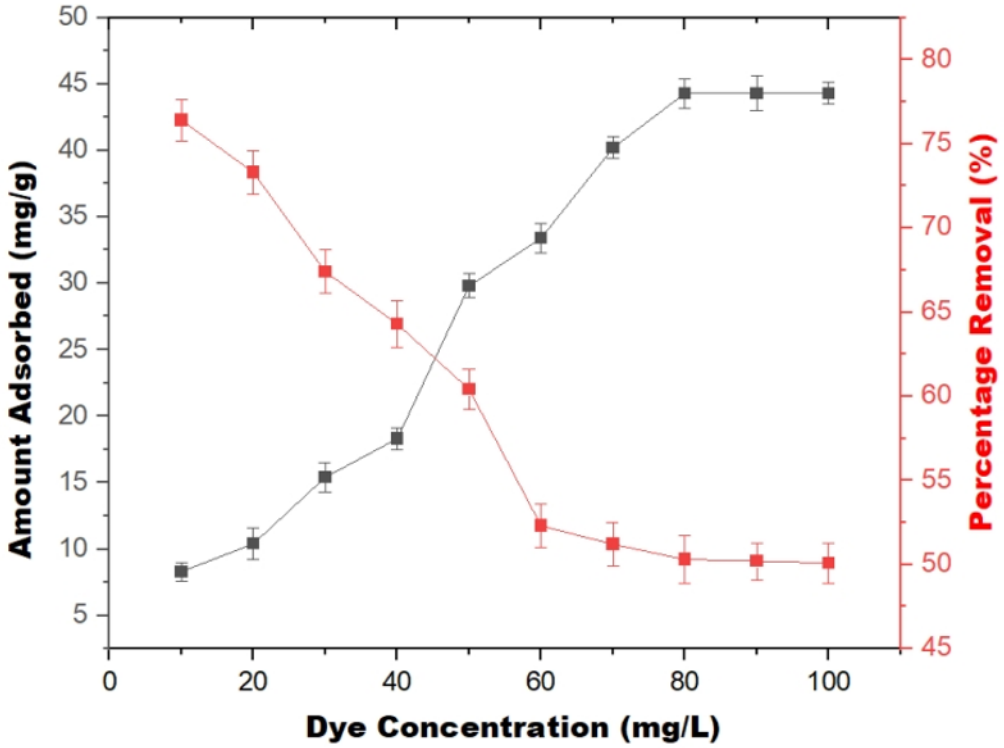


Fig. 7. Impact of adsorbent initial concentration on the removal of EY using MH biomass

Impact of Contact Time

Figure 8 demonstrates the role of contact time on the adsorption of EY dye onto MH. The results indicate that the amount of EY adsorbed increased sharply during the initial stages, with a rapid adsorption phase observed within the first 30 min, after which the curve became level at 60 min, suggesting that as the optimum uptake of 41.2 mg/g was attained at this contact time for maximum EY removal. At the preliminary stage, the sorption process was still progressing toward equilibrium because many active binding sites remain unoccupied, allowing EY molecules to diffuse quickly from the bulk solution to the adsorbent surface. As contact time increased to the optimal point, these sites progressively became occupied until near-complete saturation was achieved (Adeogun *et al*. 2018; Ofudje *et al*. 2021).

Beyond 60 min the removal efficiency remained relatively constant, indicating that the adsorption process had reached equilibrium. At this stage, all available active sites were effectively filled, and no further significant uptake occurred. The plateau in efficiency reflects a dynamic equilibrium between adsorption and desorption processes, where some dye ions may begin to detach from the adsorbent surface due to repulsive forces, competitive interactions, or saturation effects, while others continue to bind (Wang *et al*. 2020). This behavior is consistent with the adsorption studies by Uzosike *et al*. (2022), where the initial rapid phase is followed by a slower approach to equilibrium as the driving force for mass transfer diminishes in their work on the removal of bisphenol-A dye from wastewater.

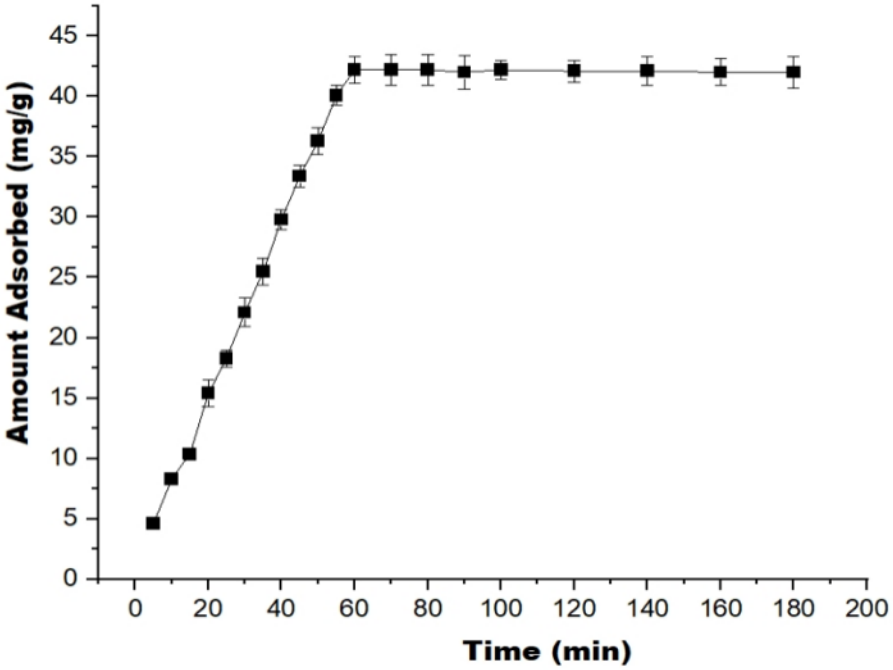


Fig. 8. Impact of contact time on the uptake of EY using MH biomass

Sorption Kinetic Studies

The linear representations of the PFO, PSO, and IPD kinetic models are displayed in Figs. 9(a–c), and the corresponding parameters are given in Table 2. Among the tested kinetic models, the PFO model provided the best fit to the experimental data, as indicated by the highest coefficient of determination (R^2 = 0.992) and closer agreement between experimental and calculated equilibrium adsorption capacities. The PSO model showed a comparatively lower fit (R^2 = 0.925), suggesting it is less representative of the adsorption kinetics in this system. In line with the observations of Hubbe *et al*. (2019), the apparent applicability of the PSO model should not be interpreted as evidence of a true second-order adsorption mechanism, but rather as a possible mathematical approximation arising from diffusion-related processes. The IPD model also fitted well with the data, with the linear plot of q_t *versus* $t^{1/2}$ showing a multi-linear profile, indicating that adsorption occurred in multiple stages, *viz.*, including both external film diffusion and intraparticle diffusion, with the boundary layer playing a significant role (Dharmarathna and Priyantha 2024; Mohamed *et al*. 2024). The intraparticle diffusion model further showed that diffusion contributed to the overall adsorption process; however, it did not solely control the rate. Thus, the adsorption kinetics were best described by the PFO model, with diffusion playing a supporting role.

Recent studies on dye or organic pollutant sorption on biomass-derived materials report that more than one kinetic model can sufficiently fit experimental data and suggest this as multi-step or mixed mechanisms. Consistent with the analysis of Hubbe *et al.* (2019), a good fit to the pseudo-second-order (PSO) model should not be interpreted as evidence of chemisorption or activation energy–controlled processes. Rather, it often reflects rate limitations associated with diffusion into a network of fine pores.

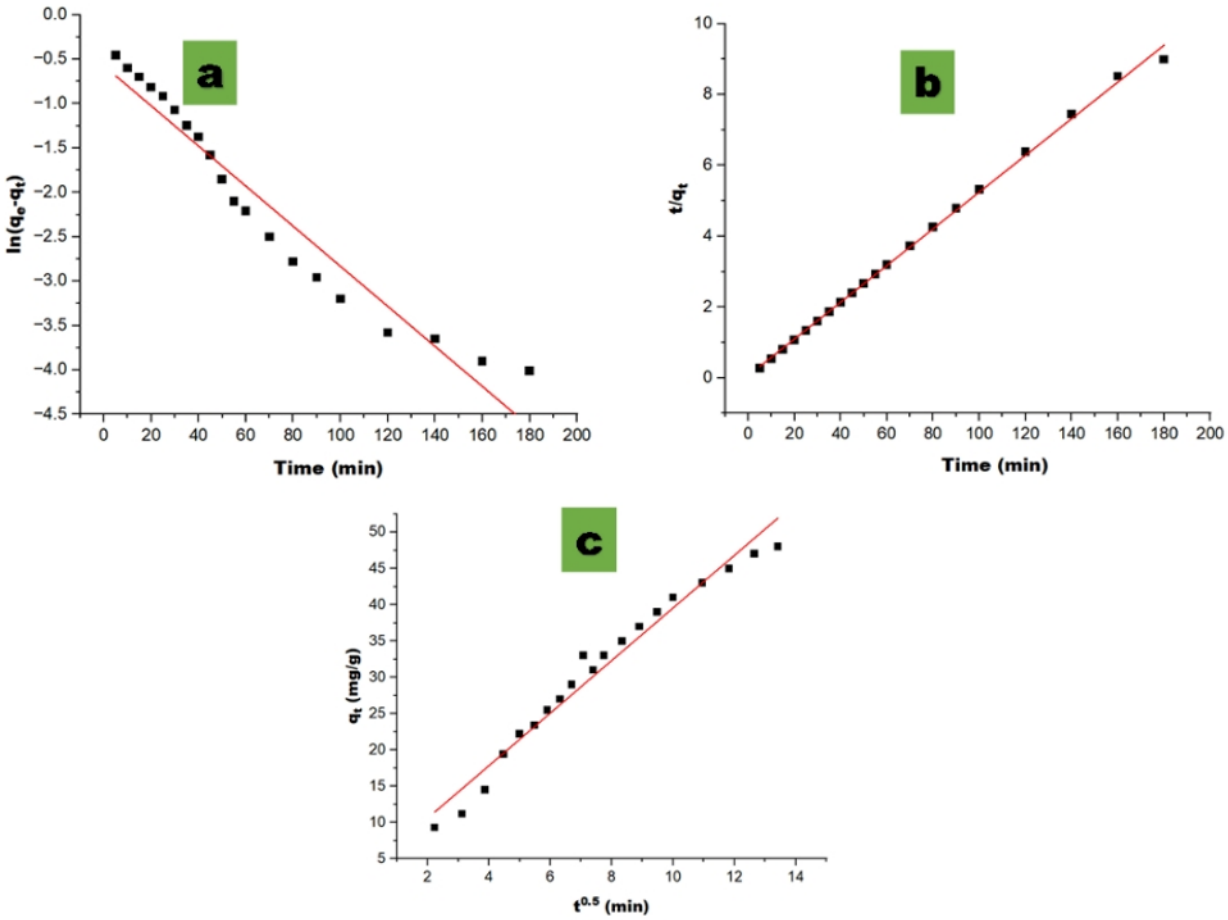


Fig. 9. Linear representations of (a) pseudo-first-order, (b) pseudo-second-order, and (c) intra-particle diffusion models for the adsorption of EY onto MH

Table 2. Kinetic Parameters for the Removal of EY using MH

Model	Kinetic Parameter	EY
Pseudo-first order	$q_{e\ (exp.)}$ (mg/g)	33.02
	$q_{e\ (cal.)}$ (mg/g)	35.31
	k_1	0.524
	R^2	0.992
	% SSE	0.008
Pseudo-second order	$q_{e\ (cal.)}$ (mg/g)	26.82
	k_2	0.108
	R^2	0.925
	% SSE	0.016
Intraparticle diffusion	K_{id}	10.45
	C	1.056
	R^2	0.968
	% SSE	0.054

In this context, the observations of Guleç *et al.* (2022), where multiple kinetic models (PFO, PSO, and intraparticle diffusion) provided reasonable fits for methylene blue adsorption onto biochars, are more appropriately interpreted as indicating the coexistence of mass transfer steps—particularly pore diffusion—alongside surface interactions, rather than distinct mechanistic regimes inferred directly from model selection. Similarly, in

studies of activated biochar for dye adsorption, the best fit was PSO kinetics, however IPD model still gave linear segments, suggesting that diffusion inside pores is operative in later stages (Pieczykolan 2025).

Adsorption Isotherm

Adsorption isotherms define the connection between the amount of solute adsorbed and that which is left at equilibrium. Figures 10(a–c) illustrates the fitting of sorption data to the Langmuir, Freundlich, and Temkin isotherm models, while Table 3 summarizes the corresponding parameters. Among the tested isotherms, the Langmuir model gave the best fit based on correlation coefficient and error analysis. Although the Langmuir model is usually associated with monolayer adsorption on a homogeneous surface, such assumptions may not strictly apply to lignocellulosic biomass materials, which are inherently heterogeneous in composition, pore structure, and surface functionality. Thus, the good agreement with the Langmuir model in this study is more appropriately viewed as an empirical indication that adsorption occurs within a finite number of energetically favorable sites under the studied conditions, rather than definitive proof of surface uniformity or ideal monolayer coverage.

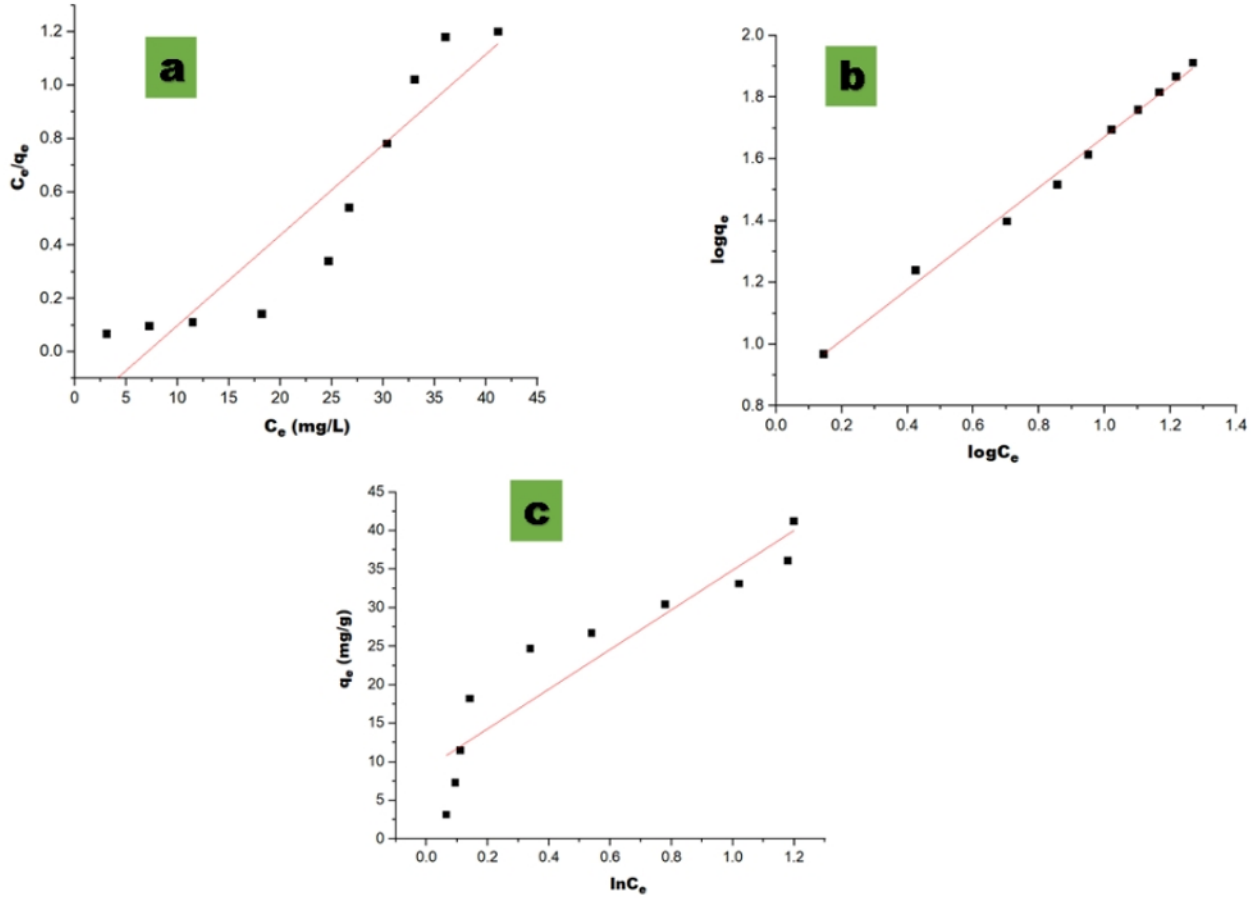


Fig. 10. Isotherm models of Langmuir (a), Freundlich (b), and Temkin (c) for the adsorption of EY onto MH

The dimensionless separation factor (R_L) value is less than 1, indicating favorable adsorption conditions (Adeogun *et al*. 2018; Ragadhita and Nandiyanto 2021). The

comparatively lower fit of the Freundlich model does not negate the presence of surface heterogeneity but may reflect the limited concentration range or experimental conditions investigated.

The Temkin model, which incorporates adsorbent–adsorbate relationships and assumes a linear decline in adsorption heat with coverage, produced an R^2 value of 0.786. The Temkin constant being greater than one indicates an endothermic adsorption process, where adsorption is favoured at higher temperatures. This report aligns with previous work on the sorption of anionic dyes onto lignocellulosic materials (Pereira *et al*. 2023).

Table 3. Parameters from Isotherm Modelling for the Adsorption of EY onto MH

	Parameters	MH
Langmuir	Q_{max} (mg/g)	44.5
	R_L	0.415
	K_L	0.141
	R^2	0.957
	% SSE	0.002
Freundlich	N	1.462
	K_F (mg/g)(mg/L)$^{-1/2}$	26.80
	R^2	0.868
	% SSE	0.040
Temkin	B (J/mol)	13.944
	A_T	1.105
	R^2	0.786
	% SSE	0.004

Table 4. Comparison of Various Adsorbents' Maximal Adsorption Capabilities for the Removal of EY

Adsorbent	q_{max} (mg/g)	Removal Efficiency (%)	pH	Dosage (g)	Initial Conc. (mg/L)	Remarks	Reference
Pineapple peels	22.01	~75	2–3	1.0	50	Raw biomass	Ugbe *et al*. (2017)
Teak leaf litter	31.64	~80	2	1.5	100	Raw biomass	Oyelude *et al*. (2017)
Cuban palm pericarp	135.32	>95	2	0.5–1.0	100	Chemically processed	Adaramola *et al*. (2024)
Date palm seeds	~30–45	~80–90	2–4	1.0–2.0	50–100	Composite system	Abdus-Salam *et al*. (2021)
Corncob (treated)	41.79	~88	2–3	1.0	100	Modified maize biomass	Song et al. (2023)
Mango leaves	39.67	~85	2	1.0	50–100	Raw biomass	Iqbal *et al*. (2023)
Mesocellular foams (MCFs)	3.96	–	6–7	–	10–50	Engineered material	Li and Zhai (2020)
Maize husk	44.5	90.3	2	1.5	100	Native, unmodified	This study

A comparison of adsorption systems (Table 4) shows that maize husk competes favorably with other absorbents in performance evaluations. A majority of the reported

adsorbents operate under acidic conditions (pH 2–3), signifying that favorable electrostatic interactions dominate anionic dye adsorption across lignocellulosic systems. Thus, the optimum pH of 2 as reported for maize husk is in alignment with literature trends rather than a distinct advantage. Relative to adsorbent classification, it is imperative to distinguish between native and modified materials. Modified adsorbents, such as synthetic mesoporous materials and treated corncob, usually achieve enhanced performance but at the expense of additional processing complexity and cost. By contrast, the maize husk employed in this study was applied in its native, unmodified form, requiring only physical processing. This represents a key practical advantage, particularly for low-resource applications. In terms of the maximum adsorption capacity, it varied greatly among the studied materials. For instance, a chemically modified Cuban palm pericarp demonstrated the highest capacity (135 mg/g). This may be attributed to chemical treatment, which likely increases surface area, pore development, and the availability of active binding sites. On the other hand, most raw biomass materials, such as teak leaf litter (31.6 mg/g), pineapple peels (22.0 mg/g), maize husk (44.5 mg/g), and mango leaves (39.7 mg/g) exhibit moderate adsorption capacities. Despite these variations in adsorption capacity, removal efficiencies across the adsorbents remained relatively high, ranging from approximately 75% to over 95%. The role played by the pH of the solution was notably consistent across most studies, with optimal adsorption occurring under highly acidic conditions (pH 2 to 3). This trend suggests that protonation of the adsorbent surface plays a vital role in the adsorption mechanism, likely enhancing electrostatic attraction between the adsorbent and the target contaminants. An exception was observed with mesocellular foams (MCFs), which operate at near-neutral pH (6 to 7) but demonstrate significantly lower adsorption capacity (3.96 mg/g), suggesting weaker affinity for the adsorbate under those conditions.

The dosage of the adsorbent also played an important role in determining performance as most of the studies use dosages between 1.0 and 1.5 g, although some variation was observed. Furthermore, other experimental conditions like initial contaminant concentration (50 to 100 mg/L) and temperature (298 K), were largely consistent across the studies. This uniformity facilitates direct comparison and indicates that most adsorbents are effective under ambient conditions, which is advantageous for practical applications. The findings underscore the potential of low-cost biomaterials, particularly maize husk and treated corncob, as viable alternatives to more complex engineered adsorbents for wastewater treatment applications.

Thermodynamic Study

The thermodynamic parameters for the uptake of EY by MH biomass are represented in Table 5 and Fig. 11. The thermodynamic parameters for the adsorption of Eosin Yellow (EY) onto maize husk (MH) reveal that the standard Gibbs free energy change ($\Delta G°$) values were negative across the studied temperature range (−0.33 to −2.55 kJ mol^{-1}), confirming that the adsorption process is thermodynamically feasible and spontaneous (Bazan-Wozniak *et al*. 2024; Hassan *et al*. 2024). However, the relatively small magnitude of $\Delta G°$ indicates that the spontaneity is weak, rather than strong, and suggests that the adsorption process proceeds without a significant energy barrier. Typically, $\Delta G°$ lower values are associated with physisorption, involving weak intermolecular forces such as van der Waals interactions, hydrogen bonding, and electrostatic attraction, whereas larger negative values are indicative of chemisorption. Therefore, the low $\Delta G°$ values obtained in this study support the conclusion that EY adsorption onto MH is predominantly governed by physical adsorption mechanisms, which

is consistent with the FTIR analysis and proposed adsorption mechanism. Furthermore, the positive enthalpy change ($\Delta H°$ = 21.05 kJ mol^{-1}) confirms that the process is endothermic (Batool *et al*. 2023; Liyanaarachchi *et al*. 2023), with the magnitude also falling within the typical range for physisorption (< 40 kJ mol^{-1}) (Al-Ghouti and Al-Absi 2020). The positive entropy change ($\Delta S°$ = 9.25 J mol^{-1} K^{-1}) indicates an increase in randomness at the solid–liquid interface during adsorption (Batool *et al*. 2023), likely due to the displacement of water molecules and increased freedom of dye molecules upon interaction with the adsorbent surface.

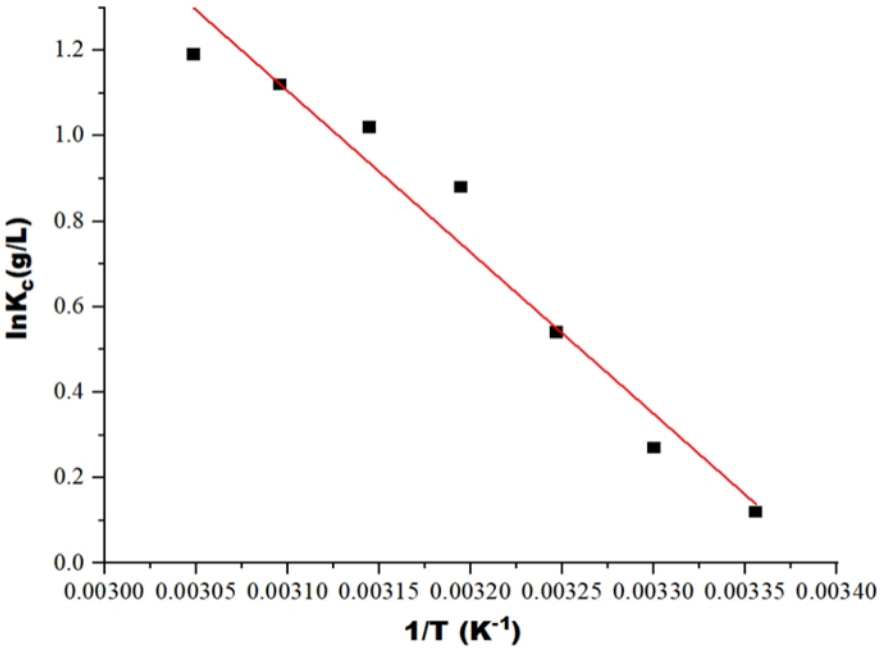


Fig. 11. Thermodynamic plot for the adsorption of EY onto MH

Table 5. Thermodynamic Parameters for the Adsorption of EY onto MH

T (K)	Δ*G* (kJ mol^{-1})	Δ*H* (kJ mol^{-1})	Δ*S* (J mol^{-1} K^{-1})
298	-0.33		
303	-0.64		
308	-0.97		
313	-1.22	21.05	9.25
318	-1.46		
323	-1.92		
328	-2.42		
342	-2.55		

Proposed Adsorption Mechanism

The adsorption of EY onto MH can be described as a multi-step process involving both chemical and physical interactions, as illustrated in Fig. 12. The adsorption of Eosin Yellow onto maize husk is likely governed by a combination of physicochemical interactions occurring at the adsorbent surface. The relatively low enthalpy changes and the presence of functional groups identified by FTIR analysis suggest that physical

interactions such as electrostatic attraction, hydrogen bonding, van der Waals forces, and π–π interactions may contribute to the adsorption process.

The analysis of equilibrium data suggests that the Langmuir isotherm gave the best representation of the adsorption data under the studied conditions, based on its higher coefficient of determination. In this context, the uptake of Eosin Yellow onto maize husk is interpreted primarily within a Langmuir-type framework, suggesting that adsorption occurs predominantly at a finite number of energetically comparable active sites with no significant interaction between adsorbed species. Surface interactions may have occurred at these active sites via electrostatic attraction, hydrogen bonding, and π–π interactions. While maize husk is structurally complex, the equilibrium behavior within the investigated concentration range appears to be adequately approximated by this simplified model.

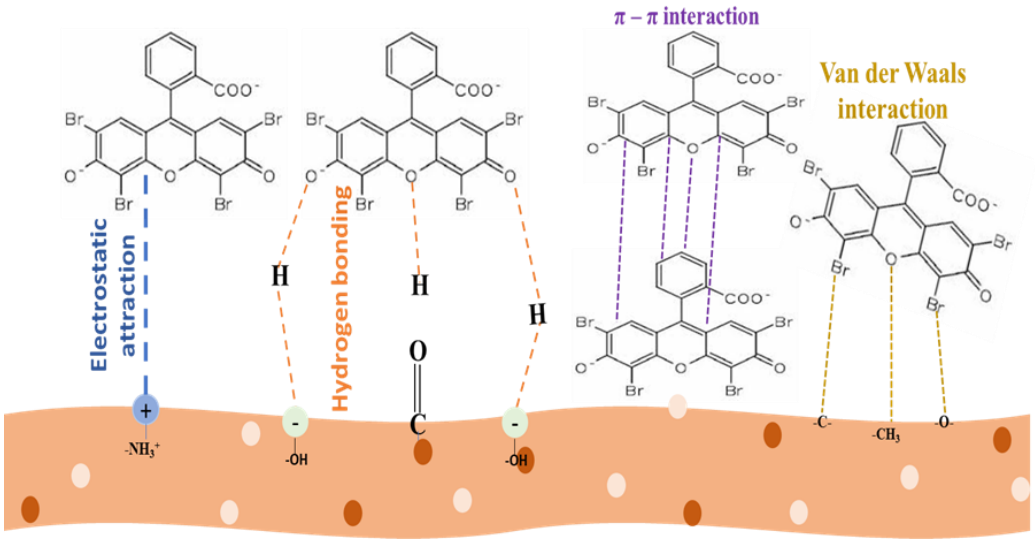


Fig. 12. Adsorption mechanism of eosin yellow dye onto maize husk

Desorption Study

The desorption–regeneration data for MH as presented in Fig. 13, reveals a progressive decline in desorption efficiency from 74.5 % (cycle 1), 74.1 % (cycle 2), 73.6 % (cycle 3), 71.2 % (cycle 4), 68.3 % (cycle 5), and 65.4 % after six cycles (cycle 6). This trend suggests that a significant fraction of the adsorbed dye is bound through reversible interactions. A progressive decline may result from incomplete desorption, partial blockage of active sites, or minor structural changes to the adsorbent surface. The relatively high initial desorption (74.5 %) may indicate that a large fraction of EY is adhered by the adsorbent as evidence from post-adsorption characterization (FTIR and SEM) infer that the adsorbent maintains its functional groups and general morphology after dye uptake, suggesting that no drastic structural degradation occurs after initial use.

Over successive cycles, a progressive decline could be due to a combination of chemical or physical alteration of surface functional groups during regeneration, incomplete dye removal after each cycle (residual dye site-blocking), and possible loss of adsorbent mass during handling/regeneration steps (Rapo *et al*. 2021). Some works achieve near-complete desorption for certain adsorbent–dye pairs using carefully chosen eluents, while other studies documented decreasing efficiency across cycles even with the same eluent due to irreversible adsorption or cumulative damage (Ramírez-Rodríguez *et al*. 2023).

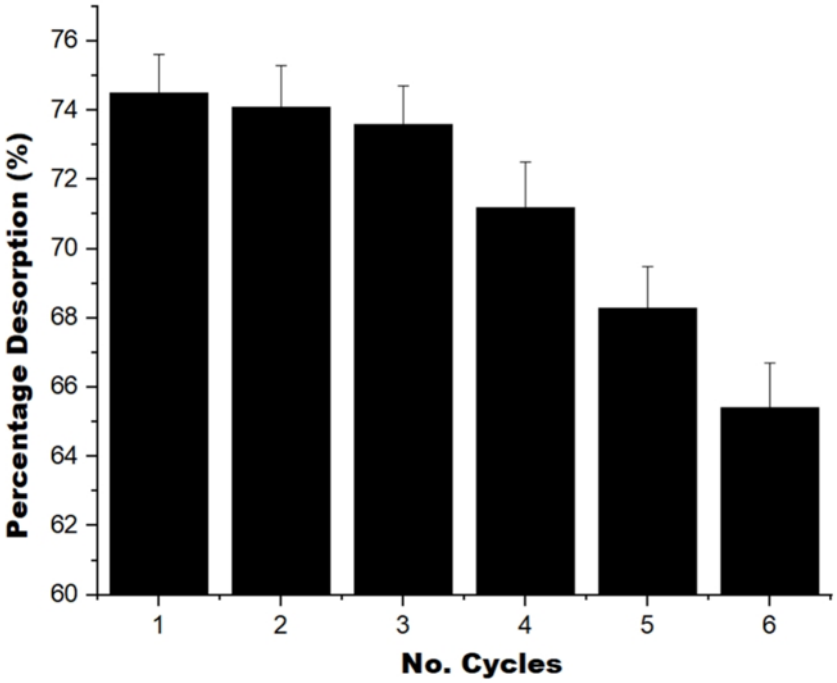


Fig. 13. Desorption plots of eosin yellow dye from maize husk

Preliminary Techno-Economic Considerations

To address the practical relevance of the developed biosorbent, a preliminary techno-economic assessment was conducted based on the experimental conditions and material preparation route employed in this study. The analysis focuses on adsorbent preparation cost, operational chemical inputs, regeneration performance, and a comparison with benchmark commercial adsorbents.

Adsorbent Preparation Cost

The preparation of maize husk (MH) involved simple physical processing steps, including washing, air-drying, grinding, and sieving, without any chemical activation or high-temperature treatment. These steps significantly reduce energy and reagent requirements compared to conventional activated carbon production. Based on typical local cost estimates for agricultural residues and small-scale processing in developing regions, the cost components are approximated as follows: raw material acquisition (negligible to minimal cost), water usage for washing, low-energy mechanical grinding, and basic handling. The total estimated preparation cost of MH is therefore in the range of 0.10 to 0.20 USD per kg of adsorbent**.** This value is substantially lower than that of commercial activated carbon, which typically ranges between 2 to 10 USD per kg**,** depending on grade and source. However, it should be noted that this estimate excludes large-scale processing, transportation, and infrastructure costs.

Adsorbent Consumption and Treatment Cost

Under the optimized conditions identified in this study (adsorbent dosage = 1.5 g per 50 mL solution), the equivalent dosage was approximately 30 g L^{-1}. Using an average preparation cost of 0.15 USD per kg, the corresponding adsorbent cost per unit volume of

treated water is estimated as 0.004 to 0.006 USD per liter of treated solution. This value represents the material cost only and does not include auxiliary operational expenses.

Chemical Consumption for pH Adjustment

The adsorption process exhibited maximum efficiency at pH 2, requiring the addition of acid (0.1 M HCl) for pH adjustment. The estimated acid consumption required to adjust near-neutral aqueous solutions to pH 2 is 2 to 6 mL of 0.1 M HCl per liter**,** depending on solution buffering capacity. Based on typical reagent costs, the corresponding chemical expense is estimated to be 0.001 to 0.003 USD per liter. While relatively modest at laboratory scale, this requirement represents an important operational consideration for large-scale implementation, as continuous pH adjustment may increase overall process cost and complexity.

Regeneration and Reusability Considerations

Desorption experiments demonstrated that MH retained appreciable regeneration capacity over multiple cycles, with desorption efficiency decreasing from 74.5% in the first cycle to 65.4% after six cycles**.** This indicates that the adsorbent can be reused, although with gradual performance decline. Assuming 5 to 6 effective reuse cycles, the effective adsorbent cost can be reduced by approximately 3 to 4 times**,** resulting in an adjusted treatment cost to approximately 0.001 to 0.002 USD per liter.

Comparison with Commercial Activated Carbon

A comparative evaluation between maize husk and commercial activated carbon is presented in Table 6.

Table 6. Preliminary Comparison of Maize Husk and Commercial Activated Carbon for Dye Adsorption

Parameter	Maize Husk (This Study)	Commercial Activated Carbon
Raw material source	Agricultural residue	Coal, coconut shell, wood
Preparation process	Washing, drying, sieving	Carbonization + chemical/thermal activation
Estimated cost (USD/kg)	0.10 to 0.20	2 to 10
Process maturity	Laboratory scale	Industrially established
Optimal pH	~2	Broad (often 4 to 8)
Adsorption capacity (mg/g)	44.5	100 to 500
Regeneration	Moderate (65 to 75% over 6 cycles)	High (often >80%)
Chemical requirement	Acidic pH + acetic acid regeneration	Variable (depends on system)

The comparison between MH and commercial activated carbon (CAC) demonstrates important trade-offs in relation to cost, performance, and practical applicability. MH, obtained from an abundant agricultural residue, offers a clear economic advantage, with an estimated cost (0.10 to 0.20 USD/kg) which is lower than that of CAC (2 to 10 USD/kg). Also, its simple preparation process, which is limited to washing, drying, and sieving, suggests minimal energy and chemical input. This makes it attractive from a sustainability perspective. However, these advantages are almost offset by notable

limitations. For instance, the adsorption capacity of MH (44.5 mg/g) is substantially lower compare with commercial activated carbon (100 to 500 mg/g), indicating that CAC remains more efficient for high-performance applications. Likewise, CAC shows superior regeneration efficiency (>80%) relative to MH (65 to 75% over six cycles), suggesting better long-term usability. Despite these shortfalls, MH shows potential as a low-cost alternative for applications where affordability and material availability are prioritized over maximum adsorption efficiency. Its moderate regeneration performance further supports its potential for reuse, although improvements in stability and adsorption capacity would be necessary for large-scale implementation.

Co-existing Ions

The role played by co-existing ions on the adsorption of Eosin Yellow is presented in Fig. 14. The results show that the presence of inorganic ions led to a decrease in adsorption efficiency compared to the control system.

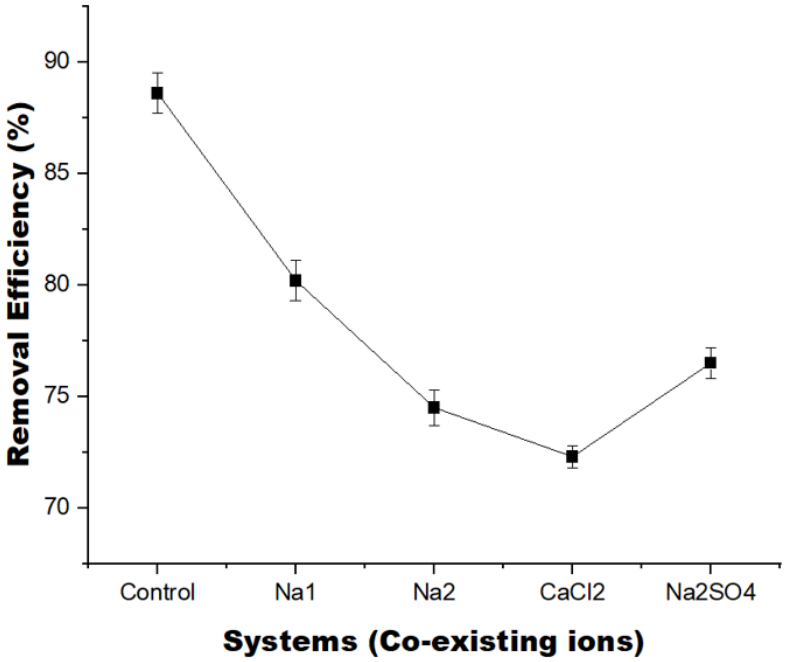


Fig. 14. Effect of co-existing ions on the removal efficiency (Note: Na1 = 0.001 M NaCl, Na2 = 0.01M NaCl)

In the presence of NaCl, a gradual decline in dye removal was noticed with increasing concentration from 0.01 to 0.1 M. This is an indication that ionic strength plays a substantial role, likely due to compression of the electrical double layer and reduced electrostatic attraction between the adsorbent surface and dye molecules. A more obvious reduction in adsorption efficiency was seen in the presence of $CaCl_2$ (0.01 M). This may be attributed to the higher charge density of Ca^{2+} ions, which enhances their ability to compete with dye molecules for available adsorption sites. Moreover, Ca^{2+} may interact more strongly with functional groups on the adsorbent surface, thus blocking active sites and reducing adsorption capacity. On the other hand, the presence of Na_2SO_4 (0.01 M) caused a moderate decline in removal efficiency, signifying that sulfate ions exert a less significant influence compared to divalent cations. This infers that cationic competition played a more dominant role than anionic effects in this system.

CONCLUSIONS

1. Native maize husk (MH) exhibited high adsorption capacity for eosin yellow (EY) dye in aqueous media, achieving significant removal under optimized operating conditions.
2. Maximum dye removal (≈90.3%) was achieved at pH 2 at 1.5 g adsorbent dosage, and 60 min contact time, showing that acidic conditions favor electrostatic attraction between protonated MH sites and anionic EY molecules.
3. Fourier transform infrared (FTIR) spectroscopy, BET surface area analysis, and scanning electron microcopy (SEM) confirmed that adsorption involved hydroxyl, carboxyl, and aromatic groups on a mesoporous surface (pore size in the range 2.8 to 3.0 nm), with visible morphological changes after dye sorption.
4. Langmuir isotherm best explained the equilibrium data ($R^2 = 0.957$, $q_{max} = 44.5$ mg/g).
5. Negative $\Delta G°$, positive $\Delta H°$, and positive $\Delta S°$ values confirmed that the process was spontaneous, endothermic, and governed by physisorption.
6. Maize husk retained substantial adsorption capacity after six regeneration cycles, demonstrating good structural stability and reusability for dye removal from aqueous systems.

ACKNOWLEDGMENTS

Authors acknowledge Princess Nourah bint Abdulrahman University Researchers Supporting Project number PNURSP2026R65, Princess Nourah bint Abdulrahman University, Riyadh, Saudi Arabia.

REFERENCES CITED

Abdus-Salam, N., Ikudayisi-Ugbe, A. V., and Ugbe, F. A. (2021). "Adsorption studies of acid dye–Eosin yellow on date palm seeds, goethite and their composite," *Chemical Data Collections* 31, article 100626. https://doi.org/10.1016/j.cdc.2020.100626

Adaramola, F., Babarinde, N., Ibikunle, A., and Osobamiro, T. (2024). "Isotherms, kinetics and thermodynamics studies on the sequestration of Eosin Yellow from aqueous solution using Cuban palm fruit pericarp as a low-cost adsorbent," *Ghana J. Sci.* 65(2), 202-227. https://doi.org/10.4314/gjs.v65i2.14

Adeogun, A. I., Ofudje, E. A., Idowu, M. A., Kareem, S. O., Vahidhabanu, S., and Babu, B. R. (2018). "Biosorption of Cd^{2+} and Zn^{2+} from aqueous solution using tilapia fish scale (*Oreochromis sp*): Kinetics, isothermal and thermodynamic study, *Desalin. Water Treat*. 107, 182–194. https://doi.org/10.5004/dwt.2018.22122

Adeoye, J. B., Balogun, D. O., Etemire, O. J., Ezeh, P. N., Tan, Y. H., and Mubarak, N. M. (2023). "Rapid adsorptive removal of eosin yellow and methyl orange using zeolite Y," *Scientific Reports* 13(1), article 21373. https://doi.org/10.1038/s41598-023-48675-4

Adeyemo, A. A., Adeoye, I. O., and Bello, O. S. (2017). "Adsorption of dyes using different types of clay: A review," *Applied Water Science* 7(2), 543-568. https://doi.org/10.1007/s13201-015-0322-y

Akhtar, N., Syakir Ishak, M. I., Bhawani, S. A., and Umar, K. (2021). "Various natural and anthropogenic factors responsible for water quality degradation: A review," *Water* 13(19), article 2660. https://doi.org/10.3390/w13192660

Aladag, E. (2023). "Optimization of nonlinear adsorption isotherm models by error analysis," *Journal of the Institute of Science and Technology* 13(1), 200-212. https://doi.org/10.21597/jist.1163166

Al-Ghouti, M. A., and Al-Absi, R. S. (2020). "Mechanistic understanding of the adsorption and thermodynamic aspects of cationic methylene blue dye onto cellulosic olive stones biomass from wastewater," *Sci. Rep.* 10, article 15928. https://doi.org/10.1038/s41598-020-72996-3

Al-Tohamy, R., Ali, S.S., Li, F., Okasha, K.M., Mahmoud, Y.A.G., Elsamahy, T., and Sun, J. (2022). "A critical review on the treatment of dye-containing wastewater: Ecotoxicological and health concerns of textile dyes and possible remediation approaches for environmental safety," *Ecotoxicol. Environ. Saf*. 231, article 113160. https://doi.org/10.1016/j.ecoenv.2021.113160

Anastopoulos, I., Karamesouti, M., Mitropoulos, A. C., and Kyzas, G. Z. (2017). "A review for coffee adsorbents," *Journal of Molecular Liquids* 229, 555-565. https://doi.org/10.1016/j.molliq.2016.12.096

Anfar, Z., Ait Ahsaine, H., Zbair, M., Amedlous, A., Ait El Fakir, A., Jada, A., and El Alem, N. (2020). "Recent trends on numerical investigations of response surface methodology for pollutants adsorption onto activated carbon materials: A review," *Critical Reviews in Environmental Science and Technology* 50(10), 1043-1084. https://doi.org/10.1080/10643389.2019.1642835

Aragaw, T. A., and Alene, A. N. (2022). "A comparative study of acidic, basic, and reactive dyes adsorption from aqueous solution onto kaolin adsorbent: Effect of operating parameters, isotherms, kinetics, and thermodynamics," *Emerging Contaminants* 8, 59-74. https://doi.org/10.1016/j.emcon.2022.01.002

Ashur, A. F., and Abbas, M. (2020). "Removal of Eosin stain from aqueous solution by rice husk," *Plant Archives* 20(2), 710-716. https://doi.org/10.31272/jeasd.conf.1.1

Batool, F., Kanwal, S., Kanwal, H., Noreen, S., Hodhod, M.S., Mustaqeem, M., Sharif, G,, Naeem, H. K., Zahid, J., and Gaafar, A. Z. (2023). "Ecofriendly synthesis of magnetic composites loaded on rice husks for acid blue 25 decontamination: Adsorption kinetics, thermodynamics, and isotherms," *Molecules* 28(20), article 7124. https://doi.org/10.3390/molecules28207124

Bazan-Wozniak, A., Jędrzejczak, A., Wolski, R., Kaczmarek, S., Nosal-Wiercińska, A., Cielecka-Piontek, J., Yagmur-Kabas, S., and Pietrzak, R. (2024). "A study on the adsorption of Rhodamine B onto adsorbents prepared from low-carbon fossils: Kinetic, isotherm, and thermodynamic analyses," *Molecules* 29(6), article 1412. https://doi.org/10.3390/molecules29061412

Bernal, V., Giraldo, L., and Moreno-Piraján, J. C. (2018). "Physicochemical properties of activated carbon: their effect on the adsorption of pharmaceutical compounds and adsorbate–adsorbent interactions," *C - Journal of Carbon Research* 4(4), article 62. https://doi.org/10.3390/c4040062

Biswas, K. (2022). "Sustainable efficacy of agriculture waste materials and the value of indigenous knowledge," *Just Agriculture* 2(11), e-ISSN: 2582-8223.

Chu, K. H. (2021). "Revisiting the Temkin isotherm: dimensional inconsistency and approximate forms," *Ind. Eng. Chem. Res.* 60(35), 13140-13147. https://doi.org/10.1021/acs.iecr.1c01788

Das, P. and Debnath, A. (2021). "Reactive orange 12 dye adsorption onto magnetically separable $CaFe_2O_4$ nanoparticles synthesized by simple chemical route: Kinetic, isotherm and neural network modeling' *Water Pract. Technol*. 16(4), 1141–1158. https://doi.org/10.2166/wpt.2021.064

de Farias, S. C. E., da Gama, B. M. V., da Silva, G. A. H., Medeiros, J. A., and de Souza, A. A. K. (2020). "Basic-dye adsorption in albedo residue: Effect of pH, contact time, temperature, dye concentration, biomass dosage, rotation and ionic strength," *Journal of King Saud University-Engineering Sciences* 32(6), 351-359. https://doi.org/10.1016/j.jksues.2019.04.006

Derayea, S. and Nagy, D. (2018). "Application of a xanthene dye, eosin Y, as spectroscopic probe in chemical and pharmaceutical analysis; a review," *Reviews in Analytical Chemistry* 37(3), article 20170020. https://doi.org/10.1515/revac-2017-0020

Dharmarathna, S. P., and Priyantha, N. (2024). "Investigation of boundary layer effect of intra-particle diffusion on methylene blue adsorption on activated carbon," *Energy Nexus* 14, article 100294. https://doi.org/10.1016/j.nexus.2024.100294

Elisa, D.-H., Marcela, G.-M., Alejandra, G.-U. J., and Elena, D.-H. M. (2022). "The nutraceutical value of maize (*Zea mays* L.) landraces and the determinants of its variability: A review," *Journal of Cereal Science* 103, article 103399. https://doi.org/10.1016/j.jcs.2021.103399

El-Rayyes, A., Arogundade, I., Ofudje, E. A., Moamen S. R., Amnah M. A., James A. A., and Sodiya E. F. (2025). "Thermodynamic, isotherm and kinetic studies lead ions adsorption onto *Manihot esculenta* chaff surface," *Sci. Rep.* 15, article 27672. https://doi.org/10.1038/s41598-025-09307-1

Faria, P. C. C, Orfão, J. J. M., and Pereira, M. F. R. (2004). "Adsorption of anionic and cationic dyes on activated carbons with different surface chemistries," *Water Research* 38(8), 2043-2052. https://doi.org/10.1016/j.watres.2004.01.034

Fashae, O. A., and Obateru, R. O. (2021). "Geospatial assessment of surface water pollution and industrial activities in Ibadan, Nigeria. in spatial modeling and assessment of environmental contaminants," *Environmental Challenges and Solutions*, P. K. Shit, P. P. Adhikary, D. Sengupta (eds), Springer, Cham. https://doi.org/10.1007/978-3-030-63422-3_12

Guleç, F., Williams, O., Kostas, E. T., Samson, A., Stevens, L. A., and Lester, E. (2022). "A comprehensive comparative study on methylene blue removal from aqueous solution using biochars produced from rapeseed, whitewood, and seaweed via different thermal conversion technologies," *Fuel* 330, article 125428. https://doi.org/10.1016/j.fuel.2022.125428

Hadad, M., Oie, C., Vo Duy, S., Sauvé, S., and Barbeau, B. (2019). "Adsorption of micropollutants present in surface waters onto polymeric resins: Impact of resin type and water matrix on performance," *Sci. Total Environ* 660, 1449-1458. https://doi.org/10.1016/j.scitotenv.2018.12.247

Hassan, I. A. H., Cihangir, N., Idil, N., and Aracagok, Y. D. (2024). "Adsorption of azo dye by biomass and immobilized Yarrowia lipolytica; equilibrium, kinetic and thermodynamic studies," *World J. Microbiol. Biotechnol*. 40(5), article 140. https://doi.org/10.1007/s11274-024-03949-5

Hemashenpagam, N., and Selvajeyanthi, S. (2023). "Textile dyes and their effect on human beings," in: A. Ahmad, M. Jawaid, M. N. Mohamad Ibrahim, A. A. Yaqoob, and M. B. Alshammari (eds.), *Nanohybrid Materials for Treatment of Textiles Dyes*, *Smart Nanomaterials Technology*, Springer, Singapore. https://doi.org/10.1007/978-981-99-3901-5_3

Hubbe, M. A., Azizian, S., and Douven, S. (2019). "Implications of apparent pseudo-second-order adsorption kinetics onto cellulosic materials. A review," *BioResources* 14(3), 7582-7626. https://doi.org/10.15376/biores.14.3.7582-7626

Ilyas, M., Ahmad, W., Khan, H., Yousaf, S., Yasir, M., and Khan, A. (2019). "Environmental and health impacts of industrial wastewater effluents in Pakistan: A review," *Reviews on Environmental Health* 34(2), 171-186. https://doi.org/10.1515/reveh-2018-0078

Iqbal, M., Zafar, S., Khan, M. I., Shahida, S., ur Rehman, H., Iqbal, M., Shanableh, A. and Javed, T. (2023). "Utilization of *Mangifera indica* leaves powder as a cost-effective adsorbent for the removal of eosin yellow from wastewater," *Desalination and Water Treatment* 306, 236-244. https://doi.org/10.5004/dwt.2023.29843

Ismail, M. S., Yahya, M. D., Auta, M., and Obayomi, K. S. (2022). "Facile preparation of amine -functionalized corn husk derived activated carbon for effective removal of selected heavy metals from battery recycling wastewater," *Heliyon* 8(5), article e09516. https://doi.org/10.1016/j.heliyon.2022.e09516

Javier-Astete, R., Jimenez-Davalos, J., and Zolla, G. (2021). "Determination of hemicellulose, cellulose, holocellulose and lignin content using FTIR in *Calycophyllum spruceanum* (Benth.) K. Schum. and *Guazuma crinita* Lam," *PLoS ONE* 16(10), article e0256559. https://doi.org/10.1371/journal.pone.0256559

Katibi, K. K., Yunos, K. F., Man, H. C., Aris, A. Z., Zuhair, M., Nor, M., Azis, R. S., and Umar, A. M. (2021). "Contemporary techniques for remediating endocrine-disrupting compounds in various water sources: Advances in treatment methods and their limitations," *Polymers* 13, article 3229. https://doi.org/10.3390/polym13193229

Kolya, H., and Kang, C.-W. (2024). "Toxicity of metal oxides, dyes, and dissolved organic matter in water: implications for the environment and human health," *Toxics* 12(2), article 111. https://doi.org/10.3390/toxics12020111

Li, X.-D., and Zhai, Q.-Z. (2020). "Evaluation of eosin Y removal from aqueous solution using nano-mesoporous material MCFs: adsorption equilibrium, kinetics, and adsorption isotherms," *Int. J. Industr. Chem.* 11(1), 55-67. https://doi.org/10.1007/s40090-020-00202-4

Lin, Q., Wang, K., Gao, M., Bai, Y., Chen, L., and Ma, H. (2017). "Effectively removal of cationic and anionic dyes by pH-sensitive amphoteric adsorbent derived from agricultural waste-wheat straw," *Journal of the Taiwan Institute of Chemical Engineers* 76, 65-72. https://doi.org/10.1016/j.jtice.2017.04.010

Liyanaarachchi, H., Thambiliyagodage, C., Lokuge, H., and Vigneswaran, S. (2023). "Kinetics and thermodynamics study of methylene blue adsorption to sucrose- and urea-derived nitrogen-enriched, hierarchically porous carbon activated by KOH and H_3PO_4," *ACS Omega* 8(18), 16158-16173. https://doi.org/10.1021/acsomega.3c00339

Mahmoodi, N. M., Taghizadeh, M., and Taghizadeh, A. (2018). "Mesoporous activated carbons of low-cost agricultural bio-wastes with high adsorption capacity: Preparation and artificial neural network modeling of dye removal from single and multicomponent (binary and ternary) systems," *Journal of Molecular Liquids* 269, 217-228. https://doi.org/10.1016/j.molliq.2018.07.108

Mittal, A., Azad, M., Jhare, D., and Mittal, J. (2013). "Adsorption of hazardous dye eosin yellow from aqueous solution onto waste material de–oiled soya: Isotherm, kinetics and bulk removal," *Journal of Molecular Liquids* 179. https://doi.org/10.1016/j.molliq.2012.11.032

Mohamed, N. S., Abbas, M., and Trari, M. (2024). "Understanding the rate-limiting step adsorption kinetics onto biomaterials for mechanism adsorption control," *Progress in Reaction Kinetics and Mechanism* 49, article 14686783241226858

Moussout, H., Ahlafi, H., Aazza, M., and Maghat, H. (2018). "Critical of linear and nonlinear equations of pseudo-first order and pseudo-second order kinetic models," *Karbala International Journal of Modern Science* 4(2), 244-254. https://doi.org/10.1016/j.kijoms.2018.04.001

Ofudje, E. A., Sodiya, E. F., Ibadin, F. H., Ogundiran, A. A., Alayande, S. O., and Osideko, O. A., (2021). "Mechanism of Cu^{2+} and reactive yellow 145 dye adsorption onto eggshell waste as low-cost adsorbent," *Chem. Ecol*. 37, 268-289. https://doi.org/10.1080/02757540.2020.1855153

Ofudje, E. A., Al-Ahmary, K. M., Alzahrani , E. A., Ud Din, S., and Al-Otaibi, J. S. (2024). "Sugarcane peel ash as a sorbent for methylene blue," *BioResources* 19(4), 9191-9219. https://doi.org/10.15376/biores.19.4.9191-9219

Oyelude, E. O., Awudza, J. A., and Twumasi, S. K. (2017). "Equilibrium, kinetic and thermodynamic study of removal of eosin yellow from aqueous solution using teak leaf litter powder," *Sci. Rep.* 7(1), article 12198. https://doi.org/10.1038/s41598-017-12424-1

Pereira, S. K., Kini, S., Prabhu, B., and Jeppu, G. P. (2023). "A simplified modeling procedure for adsorption at varying pH conditions using the modified Langmuir–Freundlich isotherm," *Appl. Water Sci.* 13(1), article 29. https://doi.org/10.1007/s13201-022-01800-6

Periyasamy, A. P. (2024). "Recent advances in the remediation of textile-dye-containing wastewater: prioritizing human health and sustainable wastewater treatment," *Sustainability* 16(2), article 495. https://doi.org/10.3390/su16020495

Pieczykolan, B. (2025). "Investigation of adsorption kinetics and isotherms of synthetic dyes on biochar derived from post-coagulation sludge," *International Journal of Molecular Sciences* 26(16), article 7912. https://doi.org/10.3390/ijms26167912

Ragadhita, R., and Nandiyanto, A. B. D. (2021). "How to calculate adsorption isotherms of particles using two-parameter monolayer adsorption models and equations," *Indonesian Journal of Science and Technology* 6(1), 205-234. https://doi.org/10.17509/ijost.v6i1.32354

Ramírez-Rodríguez, A.E., Cristiani-Urbina, E., Morales-Barrera, L., and Aranda-García, E. (2023). "Continuous successive cycles of biosorption and desorption of acid red 27 dye using water hyacinth leaves as an effective, economic, and ecofriendly biosorbent," *Bioprocess Biosyst. Eng*. 46(2), 183-193. https://doi.org/10.1007/s00449-022-02822-9

Rapo, E., and Tonk, S. (2021). "Factors affecting synthetic dye adsorption; Desorption studies: A review of results from the last five years (2017-2021)," *Molecules* Sep. 6(26), article 5419. https://doi.org/10.3390/molecules26175419

Revellame, E. D., Fortela, D. L., Sharp, W., Hernandez, R., and Zappi, M. E. (2020). "Adsorption kinetic modeling using pseudo-first order and pseudo-second order rate laws: A review," *Cleaner Engineering and Technology* 1, article 100032. https://doi.org/10.1016/j.clet.2020.100032

Sharma, A., Tomer, A., Singh, J., and Chhikara, B. S. (2019). "Biosorption of metal toxicants and other water pollutants by Corn (Maize) plant: A comprehensive review," *Journal of Integrated Science and Technology* 7(2), 19-28.

Soltani, A., Faramarzib, M. and Parsaa, S.A.M. (2021). "A review on adsorbent parameters for removal of dye products from industrial wastewater," *Water Quality Research Journal* 56(4), article 181. https://doi.org/10.2166/wqrj.2021.023

Song, Y., Chen, S., and Xu, H. (2023). "Eosin Y removal using citric acid-treated corncob," *Desalination and Water Treatment* 308, 244-251. https://doi.org/10.5004/dwt.2023.29925

Tariq, A., and Mushtaq, A. (2023). "Untreated wastewater reasons and causes: A review of most affected areas and cities," *Int. J. Chem. Biochem. Sci*. 23(1), 121-143.

Ugbe, F. A., and Ikudayisi, V. A. (2017). "The kinetics of eosin yellow removal from aqueous solution using pineapple peels," *Edorium. J. Waste Manag.* 2, 5-11. https://doi.org/10.5348/W01-2017-6-OA-2

Uzosike, A. O., Ofudje, E. A., Akiode, O. K., Ikenna, C. V., Adeogun, A. l., Akinyele, J. O., and Idowu, M. A. (2022). "Magnetic-supported activated carbon obtained from walnut shells for bisphenol-A uptake from aqueous solution," *Appl. Water Sci.* 12, 201. https://doi.org/10.1007/s13201-022-01724-1

Vigdorowitsch, M., Pchelintsev, A., Tsygankova, L., and Tanygina, E. (2021). "Freundlich isotherm: An adsorption model complete framework," *Applied Sciences* 11(17), article 8078. https://doi.org/10.3390/app11178078

Wang, L., Shi, C., Pan, L., Zhang, X., and Zou, J.-J. (2020). "Rational design, synthesis, adsorption principles and applications of metal oxide adsorbents: a review," *Nanoscale* 12(8), 4790-4815. https://doi.org/10.1039/C9NR09274A

Article submitted: February 10, 2026; Peer review completed: April 14, 2026; Revised version received: April 25, 2026; Accepted: May 3, 2026; Published: May 22, 2026.
DOI: 10.15376/biores.21.3.6267-6296